Bending behaviour of Textile Reinforced Concrete sandwich beams

Isabella Giorgia Colombo [1,*], Matteo Colombo [1], Marco di Prisco [1]

Politecnico di Milano, Department of Civil and Environmental Engineering, Piazza Leonardo da Vinci 32, 20133 Milano, Italy

Received 1 August 2014
Received in revised form 5 May 2015
Accepted 19 July 2015
Available online 28 July 2015

1. Introduction

Precast concrete sandwich panels are largely used worldwide, especially in Europe and North America, as structural and insulating walls in multi-unit residential, commercial and warehouse building [1]. These panels are generally made of two external reinforced concrete layers connected through the insulation layer by means of various type of shear connectors (e.g., concrete webs, metal connectors, plastic connectors or a combination of them).

Depending on the strength and stiffness of the shear connectors used, a sandwich behaves as fully-composite, partially-composite or non-composite panel [2]. In the first case, the connectors are able to transfer the shear forces between the two external layers, hence both of them carry the applied load acting as a compact section. When the connectors transfer a minimal part of the shear force from one external layer to the other, the system is considered non-composite: the amount of load carried by each layer, and hence the stress distribution, depends on the stiffness of the layer itself. As underlined by Einea et al. [1], in many non-composite panels the load is carried by just one concrete layer, that is considered as the structural one, while the other layer does not contribute to the strength of the panel and is used mainly for esthetic purposes, to enhance the panel durability and to encase the insulating material. Partially-composite panels lie in between these two extremes [3].

The thickness of each concrete layer depends on its structural function, the concrete cover required, the anchorage of the connectors and the finishing; however, in conventional sandwich panels, it is never smaller than 50 mm [1].

Some studies concerning the bending behaviour of sandwich panels were developed [4], paying particular attention to the relationship between the shear connectors used and the obtained composite action [5,6].

However, the high costs of full-scale testing, the difficulty in fabricating small-scale panels and the reluctance of the producers in sharing the information with their competitors lead to a lack of information on the mechanical performances of the precast concrete sandwich panels [5].

The main advantage of a sandwich solution, that is the integration between the thermal insulation and the wall structural

* Corresponding author.
E-mail addresses: isabellagiorgia.colombo@polimi.it (I.G. Colombo), matteo.colombo@polimi.it (M. Colombo), marco.diprisco@polimi.it (M. di Prisco).
[1] *URL:* http://www.dica.polimi.it.

element, has to be added to all the advantages related to the prefabrication such as quality control and fast mounting. The main disadvantages are related to the insufficient architectural design range, the clumsy appearance and the corrosion damages that, according to Hegger et al. [7], induce a decreasing in the acceptance of this technology for façade.

Moreover, the insulation efficiency of the sandwich panel depends on the thermal resistance of the insulation material, generally polystyrene or polyurethane, and this efficiency can be considerably reduced by the thermal bridges caused by the presence of the shear connectors, that can be significant especially in the fully-composite solution.

In order to exploit the advantages of a prefabricated sandwich solution while solving corrosion problems, improving the design possibility and obtaining the desired finishing, Hegger et al. [7] proposed sandwich panels with both the concrete layers made of Textile Reinforced Concrete (TRC) and pointed out the good mechanical behaviour of this solution. TRC is a composite cement-based material reinforced with glass, carbon or aramid fabrics that allows designers to obtain thin and lightweight struc-tures thanks to the high tensile resistance [8,9]; this material can be also used in the retrofitting of existing structures as repair layer with not only a strengthening [10], but also a protective function [11,12]. Considering sandwich panels, the use of TRC guarantees to significantly reduce the thickness of the layers if compared to traditional panels. Furthermore, the fine-grained concrete used in TRC allows to obtain good durability and finishing, features that are very important for façade elements.

In this paper a prefabricated façade sandwich characterized by an internal insulation layer made of expanded polystyrene foam (EPS, 100 mm thick) and by two external layers of Textile Reinforced Concrete (TRC, 10 mm thick) is considered. This sandwich solution is adopted in the external façade panel proposed for energy retrofitting of existing buildings in the framework of a more extensive research project (EASEE [13]); the maximum dimension of this panel is 1.5×3.3 m^2. The real panel is supposed to be placed on an existing wall by means of four punctual connec-tors placed near to the four corners of the panel on the short edges: the two upper connectors are aimed to resist only the wind pressure acting on the panel, while the two connectors placed at the bottom are loaded both by wind pressure and self weight of the panel. In order to prevent the thermal bridges caused by connectors, the insulating material is used to transfer the shear between the two external TRC layers; hence, in a full-scale panel designed with this technology, just few connecting devices, active only in extreme conditions (e.g., fire), must be provided to prevent the detachment between the two TRC layers. This approach to transfer the shear by means of the core material is commonly adopted for building sandwich panels characterized by polymeric or metallic external skins [14]; nevertheless, Ferrara et al. [15], Colombo et al. [16], di Prisco et al. [17], di Prisco et al. [18] and Muller et al. [19] proposed cement based sandwich elements in which advanced cementitious composites are used for the external layers and the connection between the layers is obtained only through the bond between the insulating material and the cemen-titious layer without any connector. The experimental campaign presented in this paper is aimed at identifying the behaviour of the sandwich composite investigated when a four point bending scheme is adopted. The results allow a deeper understanding of the failure mechanisms when different slenderness are considered and provide a reliable benchmark for future numerical modeling of structural elements characterized by this sandwich solution. In the paper two different geometries of the specimens are considered: the tests are carried out on 550×150 mm^2 and 1200×300 mm^2 sandwich beams, both characterized by a thickness of 120 mm and the stratigraphy described above.

2. Specimens and test description

The experimental campaign – whose results are presented in this paper – concerns the investigation on sandwich beams tested according to a four point bending scheme.

2.1. Cross-section and materials

The sandwich beams investigated are characterized by two external layers 10 mm thick made of Textile Reinforced Concrete (TRC) connected by an insulation layer of expanded polystyrene foam (EPS) 100 mm thick.

The expanded polystyrene foam used is commercially known as EPS250 and is characterized by a compressive strength of 0.25 MPa at a strain equal to 10% and by a low thermal conductivity (0.034 W/mK according to EN 13163 [20]). The elastic modulus is equal to 13.7 MPa: it was measured performing compressive tests on three $100 \times 100 \times 150$ mm^3 nominally identical specimens (Fig. 1). According to uniaxial tensile tests performed on a similar EPS [16], the tensile behaviour is expected to be elastic–brittle, with an higher strength in tension rather than in compression. The shear modulus can vary between 4.14 and 4.41 MPa for this class of expanded polystyrene foam according to ASTM C 578-92 [21].

TRC is obtained reinforcing a high strength fine grain mortar with an Alkali-Resistant glass fabric, manufactured by means of a leno-weave technique and covered with an epoxy coating.

The fabric used as reinforcement, whose geometrical and mechanical characteristics are collected in Table 1, was selected after performing several investigations aimed at optimizing the performance in terms of TRC strength and ductility, the bond between matrix and fabric, and the internal filament slip. The variables considered in the preliminary study were fabric geometry (warp and weft spacing and their cross-section), fabric weaving and fabric coating. The nominal strength of the selected fabric obtained in the warp direction is equal to 820 MPa. Further infor-mation on the testing procedure and some considerations on the results can be found in Colombo et al. [22].

The cementitious matrix used is characterized by a water to binder ratio equal to 0.225 and by a superplasticizer to cement ratio equal to 9.3%. The maximum aggregate size selected is equal to 1 mm. These properties guarantee a high flow capability and, hence, a good bond between matrix and fabric and the possibility to cast the mortar in pressure.

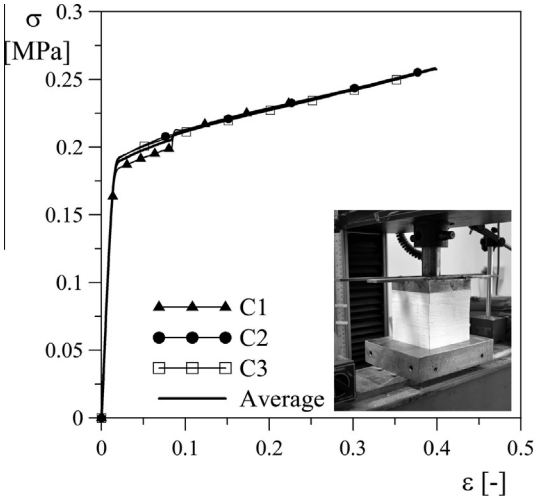

Fig. 1. EPS behaviour in compression.

Table 1
Characteristics of the fabric.

Warp wire spacing (mm)	4.9
Weft wire spacing (mm)	10.1
Warp (Tex)[a]	2 × 1200
Weft (Tex)[a]	1200
Max. tensile load for width = 70 mm (kN)[b]	11.02
STD %	6.52

[a] 1 Tex = 1 g/km.
[b] Average value of 10 tensile tests.

The in pressure casting technique (Fig. 2) is adopted in order to minimize the voids (defects) in the mortar and to enhance the bond between TRC layers and EPS, also because just the insulating material is used to transfer the shear between the external TRC layers. A proper formwork characterized by transparent walls was built in order to check by visual inspection the injection of the mortar (Fig. 2a). An EPS layer with an AR-glass fabric fixed on each side is first placed into the formwork. This EPS prism was simply cut from a larger block and no particular surface treatment was performed. After mixing, the fresh mortar is allowed to flow into a tank (Fig. 2b), that, once filled, is closed (Fig. 2c) and then pressurized. In this way the mortar can be injected in the formwork from the bottom through a spherical valve (Fig. 2d). 48 h after casting, specimens are demoulded and then cured in air at least for 28 days before testing.

The mortar is characterized by a bending tensile strength (f_{ctf}) equal to 13.5 MPa and by a cubic compressive strength (f_{cc}) equal to 73 MPa; these mechanical properties are determined according to EN 196-1 Standard for mortar [23] considering two and four nominally identical specimens respectively for bending and compression.

2.2. Geometry and test set-up

Four point bending tests are performed on sandwich beams using an electromechanical press INSTRON 5867 with a maximum load capacity of 30 kN. Two specimen geometries are taken into account: a small beam (550 × 150 × 120 mm^3; identified by "S" letter) and a larger one (1200 × 300 × 120 mm^3; identified by "B" letter). In all cases the warp of the glass fabric is aligned with the beam longitudinal direction. The specimen geometries and the test set-ups are shown both for small and big specimens respec-tively in Fig. 3a and b; the measured cross-section sizes of each specimen are summarized in Table 2, in which specimen width (b) and height (h) as well as the thickness of the two TRC layers (h_{TRC}^{sup} and h_{TRC}^{inf}) are collected. Metallic plates, respectively 50 and 80 mm wide for "S" and "L", are glued on each specimen over the supports and under the knives through which the load is applied in order to reduce stress concentration. The loading and the supporting cylinders have a diameter equal to 40 mm and are free to rotate on their axis and in the plane perpendicularly to the longitudinal axis of the specimen.

As shown in Fig. 4, each specimen is instrumented with the following displacement transducers:

- LVDT1 and LVDT2 are placed in vertical position on the front side of the specimen and are aimed at measuring the specimen deflection under the loading knives (δ_1 and δ_2). The measured values δ_1 and δ_2 are the relative displacements of points B1 and B2 with reference to point A (Fig. 4b). δ_{inf} is obtained as the mean value of δ_1 and δ_2.
- LVDT3 and LVDT4 are placed in vertical position on the rear side of the specimen and are aimed at measuring the deflection of the upper TRC layer under the loading knives (δ_3 and δ_4). δ_3 and δ_4 represent the relative displacement of points C1 and C2 with reference to point A. δ_{sup} is obtained as the mean value of δ_3 and δ_4.
- LVDT5 is placed on the upper TRC layer with a gauge length defined as L_{sup} (Table 2) in order to measure the superior longitudinal displacement (δ_{compr}) on the compressed side inside the constant bending moment region.
- LVDT6 and LVDT7 are placed on each side of the lower TRC layer astride the constant bending moment region with a gauge length defined respectively as L_{inf1} and L_{inf2} (Table 2) for LVDT6 and LVDT7. These transducers are instrumental to mea-sure the crack opening displacement (COD) on both the front (COD1) and the rear (COD2) sides.

In order to not affect the deflection measures δ_{inf} and δ_{sup} by the crushing of the material at the supports, a proper frame is used. Two C profiles are placed on the upper surface of the specimen over the supports; on these profiles, two aluminum bars, carrying the transducers LVDT1, LVDT2, LVDT3 and LVDT4, are placed. All the transducers used are inductive full bridge type, with a nominal displacement equal to 10 mm, with the exception of the LVDT5 employed in the case of small specimens, that is an inductive half bridge with a nominal displacement of +/−1 mm. The data acquisition is performed by using the electronic measurement system SPIDER8 by HBM. Each instrument has been removed from the specimen once reached its maximum displacement.

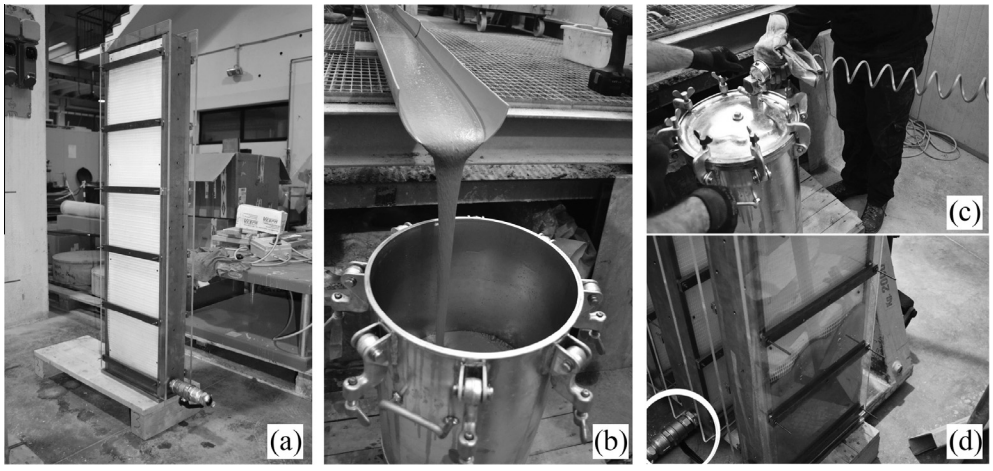

Fig. 2. Casting of the sandwich beams: formwork with the EPS panel and the fabrics placed inside (a), tank filling (b), tank closure (c) and in-pressure injection of the mortar inside the formwork (d).

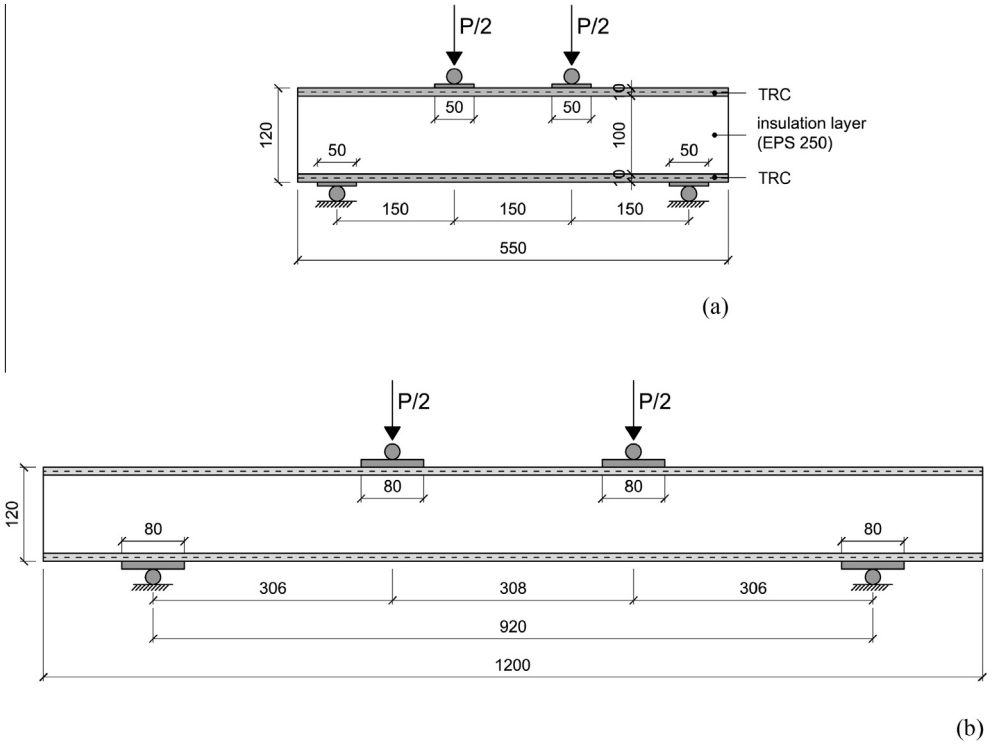

Fig. 3. Sandwich beam geometry and test set-up (measures in mm): small "S" (a) and big "B" (b) specimen.

Table 2
Sandwich beams: sizes, peak load and corresponding vertical stroke, lengths of the gauges.

Specimen	b (mm)	h (mm)	$h_{TRC\ sup}$ (mm)	$h_{TRC\ inf}$ (mm)	P_{max} (kN)	$stroke_{max}$ (mm)	L_{sup} (mm)	L_{inf1} (mm)	L_{inf2} (mm)
S1	147.5	122.0	11.8	9.7	7.66	30.31	51.0	195.0	195.0
S2	150.5	121.4	10.5	11.4	9.01	58.33	51.0	202.0	200.0
S3	150.2	122.2	9.7	12.0	9.19	79.85	53.0	201.5	201.0
S4	147.8	121.5	11.5	9.5	8.68	76.82	49.0	199.0	201.0
B1	302.5	121.8	9.9	11.7	16.31	41.91	100.0	399.0	395.0
B2	304.5	121.8	10.8	10.6	10.27	7.99	102.0	399.5	400.5
B3	300.5	121.2	11.7	8.4	16.38	52.99	103.0	399.0	402.0
B4	302.0	121.1	8.7	11.6	15.74	42.97	103.0	403.5	403.0

Four nominally identical tests were performed for both small and big specimens. Fig. 5 shows a small and a big specimen during a test. The tests are displacement-controlled, considering the machine crosshead displacement (stroke) as feedback parameter and are performed by imposing an initial stroke rate of 1E-3 mm/s. After crack formation, in the second phase of the test, the rate is increased up to 4E-3 mm/s.

3. Experimental results

The results are shown in Figs. 6 and 7 respectively for small and big specimens in terms of load vs. stroke and bending moment vs. nominal curvature curves. The bending moments are obtained by multiplying the load acting on one knife for the lever arm, while the nominal curvature is defined as:

$$\vartheta = \frac{\varepsilon_{inf} + \varepsilon_{sup}}{h} \text{ with } \varepsilon_{inf} = \frac{1}{2}\left(\frac{COD1}{L_{inf1}} + \frac{COD2}{L_{inf2}}\right) \text{ and } \varepsilon_{sup} = \frac{\delta_{compr}}{L_{sup}} \quad (1)$$

The values of δ_{compr}, COD1 and COD2, measured through the displacement transducers LVDT5, LVDT6 and LVDT7, are corrected before computing the curvature by taking into account that each instrument is not placed exactly on the specimen surface, but it is located at a certain distance. To correct these measures a rigid rotation assumption is considered.

Figs. 8–10 show the pictures of the specimens after test both for small and big specimens.

Looking both the load–stroke curves and the pictures, it is worth noting that the test on specimen S1 was stopped due to external causes before reaching the failure, while specimen B2 presented an early shear failure due to the presence of a small con-nector used to fix the fabric to the insulation material, that acted as a local defect in the EPS. Besides, in the case of specimen B1, a knife release occurred, causing the upper TRC punching.

Considering the load–stroke graphs, in both cases the results are characterized by a good repeatability, especially in the initial phase; the scatter remains very limited also in the second branch of the curve (st. dev. less than 5%). The maximum load (P_{max}) reached by each specimen, together with the corresponding displacement ($stroke_{max}$), is summarized in Table 2.

Considering small specimens (Fig. 8), it is possible to observe that multi-cracks occurred in both the upper and the lower TRC layers, hence the specimen behaves as a partially composite panel [1], mainly because of the low stiffness of the EPS. In the upper TRC face the multi-cracking took place under the plates used to distribute the load and to reduce stress concentration. Looking at the lower TRC

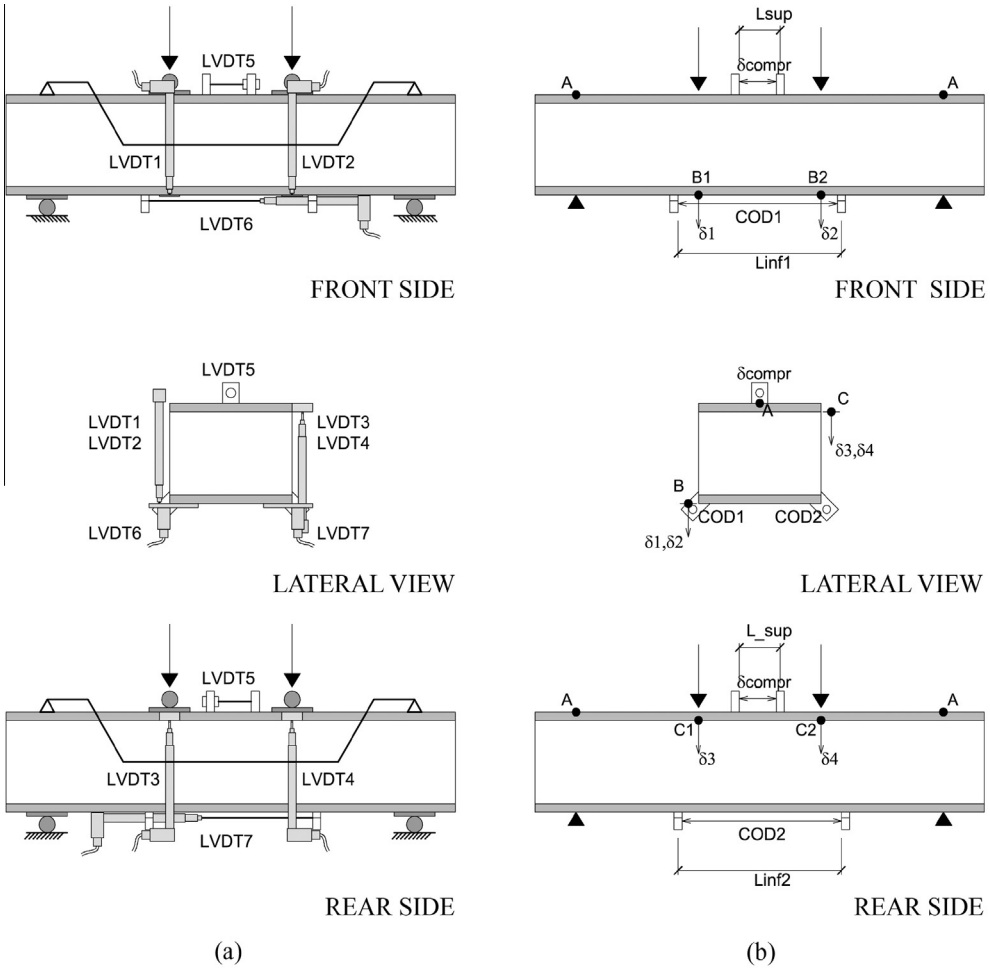

Fig. 4. Geometry of the instrumented sandwich beam (a) and measures read by the instruments (b).

Fig. 5. Specimens during testing: small "S" sandwich beam (a) and big "B" sandwich beam (b). Pictures taken after the removal of the transducers.

face, it is possible to note that, even if the multi-cracking phenomenon occurred in all the specimens, in cases S1 and S2 cracks are quite close (cracking space equal to about 15 mm), while in cases S3 and S4 only few larger cracks developed. The difference in the crack pattern may be related to the fabric position inside the lower TRC layer. As a matter of fact, specimens that experienced a more dense crack pattern (S1 and S2) are characterized by the fabric placed in the middle of the layer or closer to the external surface. For the situations in which the fabric remained close to the EPS (S3 and S4), a larger crack distance is observed. However, the ultimate failure mechanism is the same in all the cases and the global response is characterized by a good repeatability. Taking a careful look to the crack pattern of specimens S1 and S2, it is possible to observe that cracks are not symmetric with respect to the longitudinal axis: this lack of symmetry may be due to a small penetration of mortar on just one of the lateral side of the specimen, thus creating a very thin (less than 1 mm) lateral layer of mortar on just a portion of the side itself. This thin layer causes a difference in the stiffness between rear and front side, thus compromising the symmetry of the crack pattern. The ultimate failure of the small specimens (specimens S2, S3 and S4) occurred when the tensile failure of the lower face is achieved, even if the mechanism that mainly contributes to the non-linear behaviour of the response is the plastic shear deformation of the core.

Looking at crack patterns in Fig. 10, also big specimens behave as partially composite panels since they present the multi-cracking

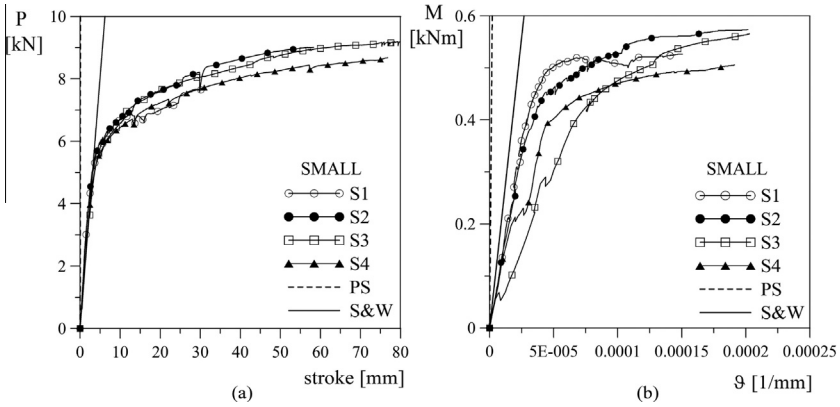

Fig. 6. Test results: load vs. stroke (a) and bending moment vs. nominal curvature (b) curves for small "S" specimens.

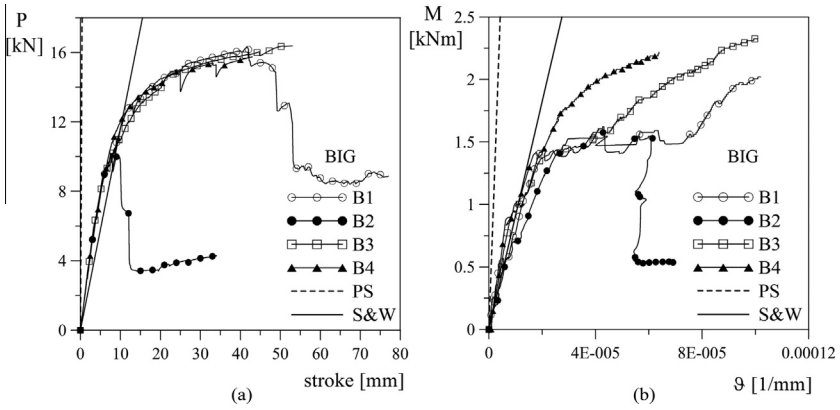

Fig. 7. Test results: load vs. stroke (a) and bending moment vs. nominal curvature (b) curves for big "B" specimens.

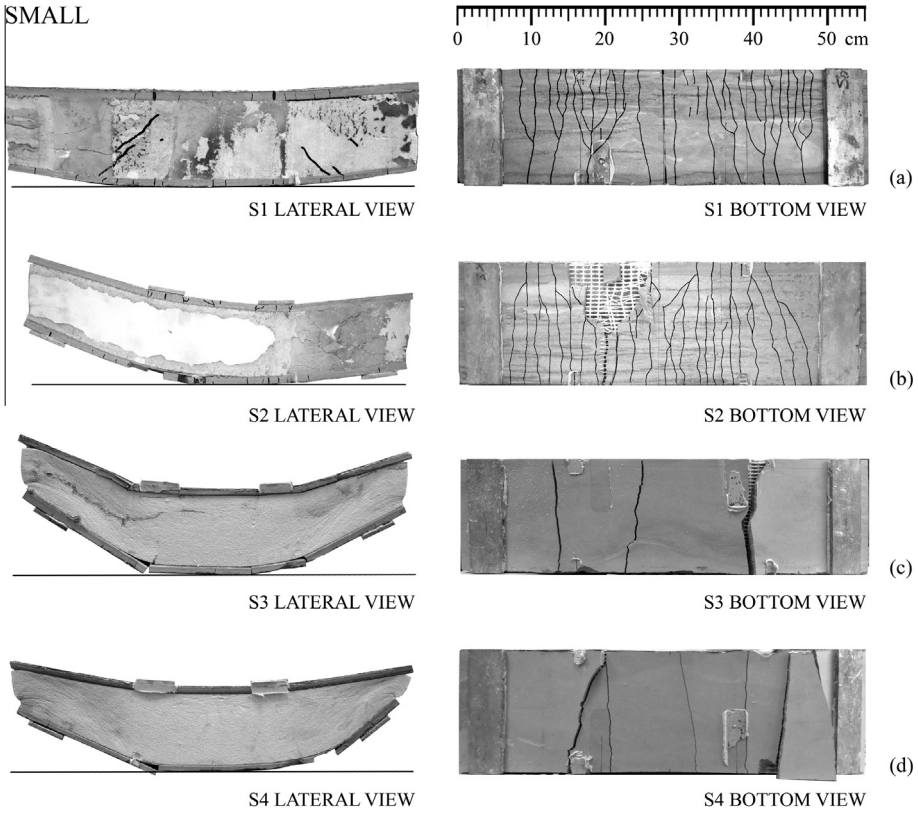

Fig. 8. Lateral and bottom view of small "S" specimens after test: S1 (a), S2 (b), S3 (c) and S4 (d).

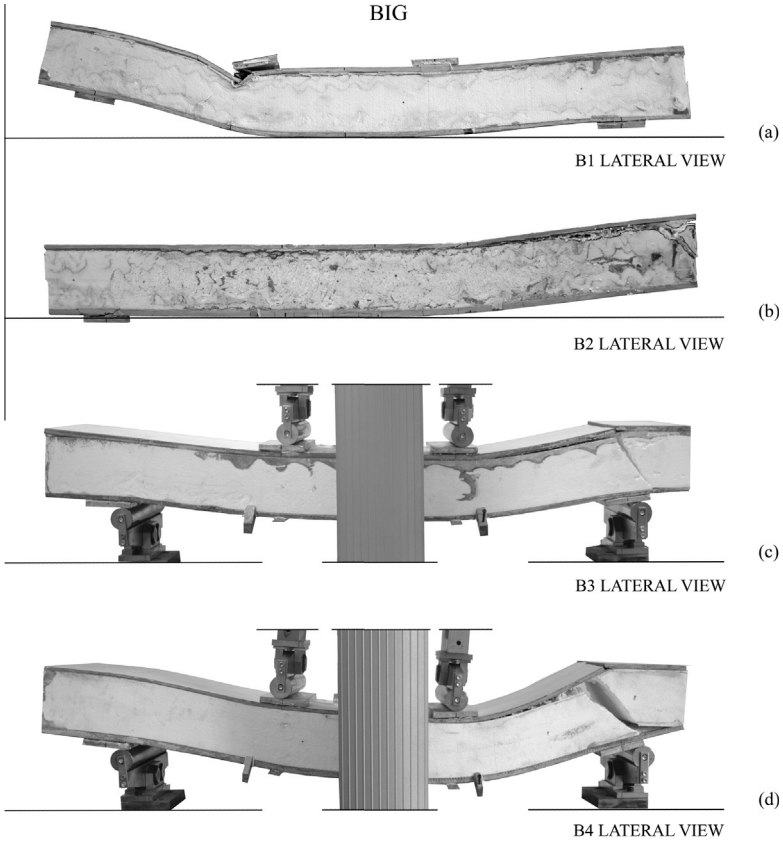

Fig. 9. Failure mode of big "B" specimens: B1 (a), B2 (b), B3 (c) and B4 (d).

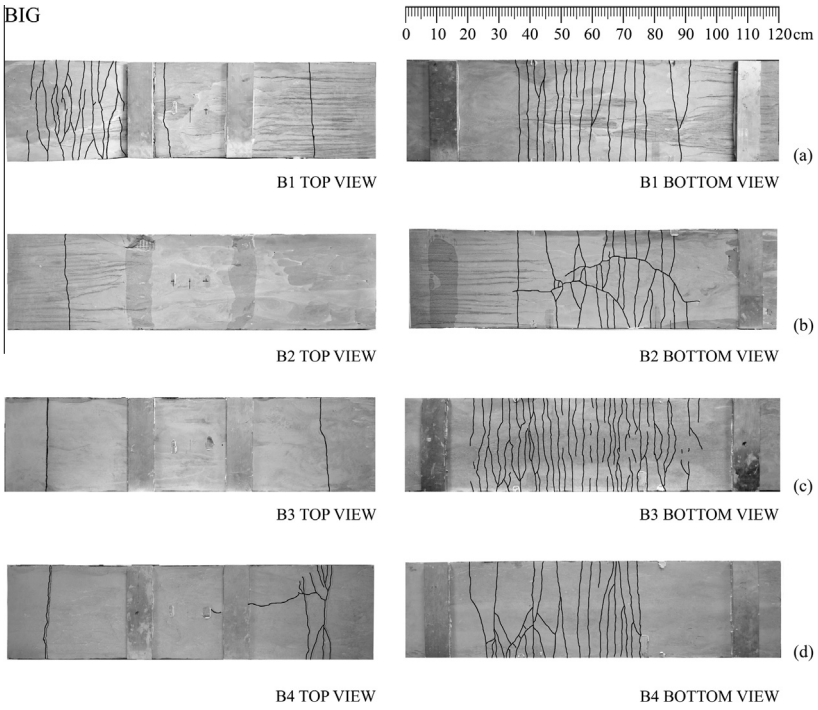

Fig. 10. Crack pattern of big "B" specimens on the top and bottom sides: B1 (a), B2 (b), B3 (c) and B4 (d).

phenomenon on both the TRC layers; some differences can be identified if the behaviour is compared with the small specimen one. First of all, even if the shear band formation in EPS is noticeable and contribute to the non-linearity of the response, the bending behaviour is more important if compared with the small specimens. Some cracks appear also on the upper surface of the specimens (Fig. 10 – top view), thus indicating that tensile stresses arise on the extrados of the upper TRC layer close to the supports.

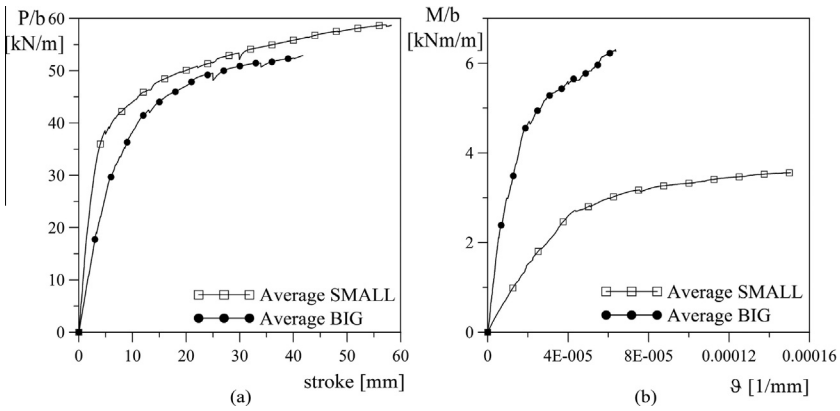

Fig. 11. Test results: specific load vs. stroke (a) and specific bending moment vs. nominal curvature (b) average curves.

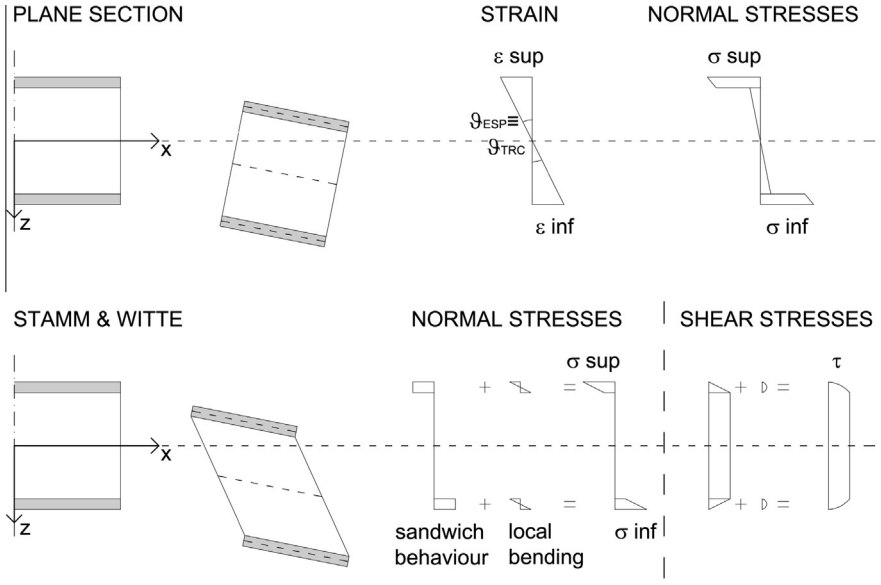

Fig. 12. Assumptions of the analytical solutions adopted to predict the elastic behaviour of the sandwich beams: plane section (PS) and Stamm & Witte (S&W) models.

These tensile stresses can be justified considering the upper TRC layer as a thin beam laying on a continuous deformable support that experiences a negative (upper surface in tension) bending moment close to the supporting cylinders. In both the big specimens that reached the ultimate failure (B3 and B4), this is governed by the development of a shear crack in the EPS layer over one support (Fig. 9). The main shear crack also propagates longitudinally along the specimen, leading to the debonding between TRC and EPS.

The load vs. crosshead displacement of the two different solutions is compared in Fig. 11a by normalizing the applied load with the specimen width. The average curves of nominally identical tests for each solution are reported in this figure. It is worth noting that both the solutions are characterized by a comparable behaviour and, in particular, the final plastic branch is very similar, thus indicating that the shear behaviour of both the solutions plays a key role in the overall response of the specimens.

Concerning the moment vs. nominal curvature behaviour of the two solutions investigated (Figs. 6b and 7b), it is important to underline that each curve is stopped when one of the displacement transducers involved in the computation of the curvature (LVDT5, LVDT6 or LVDT7) reached its maximum displacement, that always happened before the ultimate failure of the specimens.

The two solutions are compared in Fig. 11b in terms of specific moment vs. nominal curvature, where the specific moment is computed by dividing the bending moment by the specimen width. The curves plotted are the average curves of nominally identical specimens. It is worth to remind that the nominal curva-ture is computed in the constant bending moment region between the loading knives. Large differences between the two solutions can be observed: the final plastic branch is characterized by a larger specific moment value in the case of big specimens, thus indicating a more significant contribution of bending. Even the initial stiffness of the two average curves is quite different. In order to better discuss this difference, two analytical solutions for the elastic behaviour of sandwich beam are adopted to predict the initial elastic stiffness of the two specimen geometries (with TRC still uncracked): the plane section (PS) approach and the Stamm & Witte (S&W) model [24]. In both cases linear elastic materials, perfect bond between the EPS and the TRC layers, no compressibil-ity of the sandwich beam and small displacement and strain are considered.

The first model is based on the assumption that the section remains plane and, hence, there is a linear strain distribution over the cross section ($\vartheta_{EPS} = \vartheta_{TRC}$, Fig. 12); the shear deformations (γ_{xz}, considering x as the longitudinal axis and z the vertical one) of both TRC and EPS layers are assumed to be negligible. The elastic stress distribution over the cross-section is reported in Fig. 12.

The second model, proposed by Stamm and Witte in 1974 [24], is based on the following assumptions (Fig. 12):

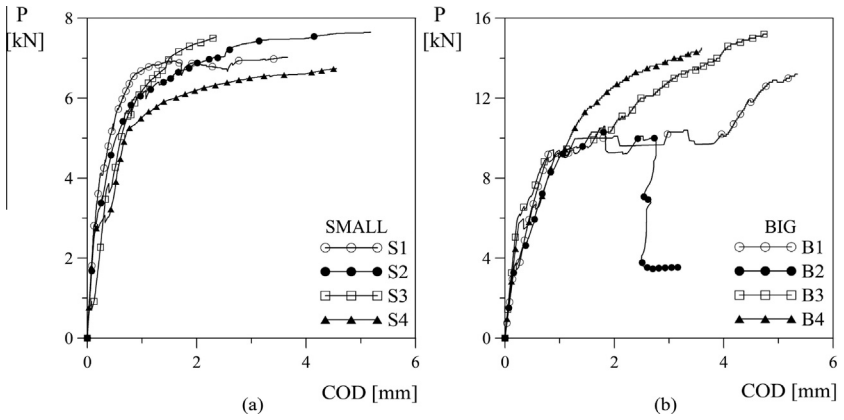

Fig. 13. Test results: load vs. crack opening displacement curves for small "S" (a) and big "B" (b) specimens.

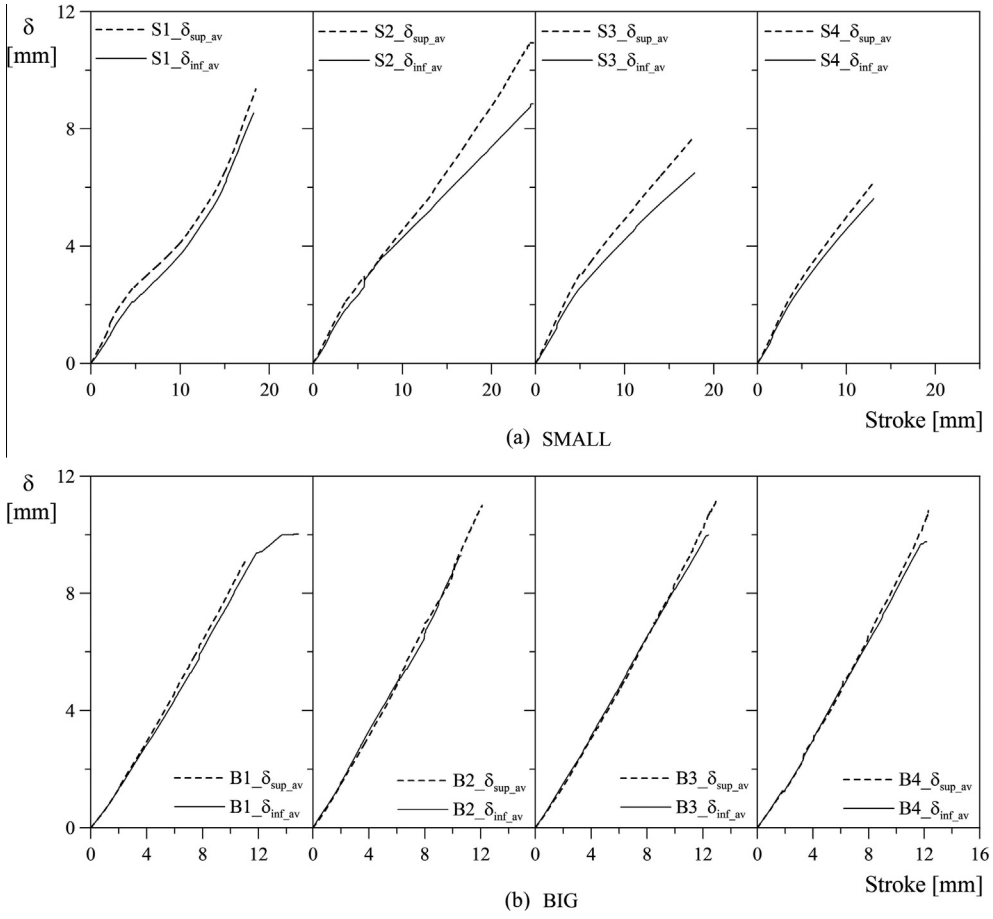

Fig. 14. Test results: superior and inferior displacement vs. stroke curves for small "S" (a) and big "B" (b) specimens.

- the EPS core is soft if compared with the outer TRC layers, hence σ_x^{EPS} can be taken equal to zero while τ_{xz}^{EPS} is constant;
- the bending stiffness of the outer TRC layers is not negligible if compared to the one of the whole sandwich beam, hence the membrane state of stress of these outer layers due to sandwich global behaviour has to be superimposed on the local bending state of each external layer;
- the shear stiffness of the outer TRC layers is large, hence TRC shear deformations γ_{xz}^{TRC} can be neglected; the cross sections of the outer layers thus remain planar and perpendicular to the axis even after the deformation (Bernoulli hypothesis);
- due to the shear deformation of the EPS core, the total cross section of the sandwich beam is not flat, but it deforms to a broken line.

The results obtained for the two different models are plotted in Figs. 6 and 7 respectively for small and big specimen solutions. An elastic behaviour is considered in both the models: an elastic modulus of 13.7 MPa is adopted for EPS according to experimental results, while a value of 30 GPa is considered for the TRC according to literature results on cement matrix characterized by similar compressive strength and maximum aggregate size [25]. Just in

the case of S&W model, a EPS shear modulus equal to 4.14 MPa is assumed (lower value proposed by ASTM C 578-92 [21] for this class of EPS).

Looking at the results, it is clear that the plane section assumption, that neglects the EPS shear deformability, is not able to provide a reliable prediction of the sandwich stiffness. Only considering the behaviour of a partially composite beam, as suggested by Stamm and Witte [24], it is possible to predict the initial linear global response of the composite both in terms of vertical displacement and nominal curvature. It is worth to note that the nominal curvature of the models was computed in the same way used for experimental results (Eq. (1)) once the strain of TRC at the extrados and at the intrados of the specimen is known. The reliability of the S&W approach allows us to conclude that the difference observed in Fig. 11b is mainly related the EPS shear deformability. Furthermore, the large difference between PS and S&W approaches is more pronounced in the case of small specimens, thus confirming the most important shear deformation contribution in this case.

The behaviour of the two different geometries tested is represented in Fig. 13 by means of the load vs. crack opening displacement (COD) curves; the large COD measured are representative of the multicracking pattern experienced by the lower TRC layer. It is important to note that the cracking of the lower TRC layer does not clearly correspond to a significant non-linearity in the global response of both the specimen geometries considered; as a matter of fact, when a COD measure of 0.5 mm is read, the TRC is clearly cracked, but the global load vs. COD curve is still linear. It is also worth to note that typical multi-crack formation branch available in the classical uniaxial tensile response of a TRC [26] is not observable in the global response of the specimens, maybe due to a stabilization effect given by both the EPS and the sandwich behaviour.

Finally, Fig. 14 presents the measurements of the different vertical displacements under the loading knives for each test. δ_{sup_av} represents the average between the top layer displacements (δ_3 and δ_4), while δ_{inf_av} is the mean value of the bottom layer displacements (δ_1 and δ_2). It is clear that, since the beginning, small specimen experiences a larger transverse compression (ε_z) of the EPS, thus indicating that this specimen mainly behaves as a 2D body and that the 1D beam assumption ($\varepsilon_z = 0$) is not reliable for this geometry. This transverse compression can be also clearly observed in the deformed shape at failure (Fig. 8), especially on the lateral part of the specimen.

On the contrary, negligible transverse strain (ε_z) can be observed for big specimens, indicating that for larger span two dimensional effect disappears and the sandwich solution respects the 1D beam assumption.

4. Conclusions

The experimental campaign presented in this paper allows us to draw some conclusions on the behaviour of the multilayered sandwich solution adopted when a four point bending scheme is considered.

First of all, considering both the geometries investigated, a large ductility is experienced in both the cases (big: $\delta_u/\delta_I = 10$; small: $\delta_u/\delta_I = 20$); this ductility is achieved by means of both large compressive plastic strain in the EPS central core and multicracking pattern in the TRC layers.

The multicracking pattern seems to be affected, especially in the small geometry, by the fabric position in the TRC layer thickness; nevertheless the different crack pattern does not affect the global response of the specimen. This consideration may lead to conclude that fabric position is more important at Serviceability Limit State (SLS), when crack opening displacements are regarded, rather than at the Ultimate Limit State (ULS), when the maximum bearing capacity is considered.

Comparing the initial response of the two different geometries with some analytical solutions for sandwich, it clearly appears that an important contribution to the global response is given by the large shear deformability of the EPS, that also causes the solution to behave as a partially composite sandwich.

The big influence of the EPS shear behaviour cannot be only observed in the first linear phase, but it is also clear in the final non-linear response, where the EPS shear seems to play a key role. This can be observed by comparing the normalized load and the normalized bending moment for both the geometries (Fig. 11a and b).

Even if the non-linear global response is strongly driven by the EPS plastic compressive strains, the specimen failures are respectively related to the tensile failure of TRC for small specimens and to the EPS brittle cracking in the case of bigger geometry.

Finally, the transverse (z direction) behaviour of the sandwich is less important for larger specimens. In this case, when the slenderness is higher, the mono-dimensional beam assumption ($\varepsilon_z = 0$) seems reliable. On the contrary, for small specimens, not negligible transverse strain ε_z denotes a two dimensional behaviour of the samples.

Acknowledgments

The authors would like to thank Gavazzi company for supplying the AR glass fabrics. The research was financially supported by the European "EASEE" project, Grant Agreement No.: 285540, Thematic Priority: EeB.NMP.2011-3 – energy saving technologies for buildings envelope retrofitting, starting date of project: March 1st, 2012, duration: 48 months.

References

[1] A. Einea, D.C. Salmon, G.J. Fogarasi, T.D. Culp, M.K. Tadros, State-of-the-art of precast concrete sandwich panels, PCI J. 36 (1991) 78–92.
[2] D.C. Salmon, A. Einea, M.K. Tadros, T.D. Culp, Full scale testing of precast concrete sandwich panels, ACI Struct. J. 94 (1997) 354–362.
[3] G. Metelli, N. Bettini, G. Plizzari, Experimental and numerical studies on the behaviour of concrete sandwich panels, Eur. J. Environ. Civil Eng. 15 (10) (2011) 1465–1481.
[4] F. Gara, L. Ragni, D. Roia, L. Dezi, Experimental behaviour and numerical analysis of floor sandwich panels, Eng. Struct. 36 (2012) 258–269.
[5] A. Benayoune, A. Samad, D. Trikha, A. Ali, S. Ellinna, Flexural behaviour of precast concrete sandwich composite panel – experimental and theoretical investigations, Constr. Build. Mater. 22 (2008) 580–592.
[6] C. Naito, J. Hoemann, M. Beacraft, B. Bewick, Performance and characterization of shear ties for use in insulated precast concrete sandwich wall panels, J. Struct. Eng. 138 (2011) 52–61.
[7] J. Hegger, and M. Horstmann, Light-weight TRC sandwich building envelopes, in: Excellence in Concrete Construction through Innovation – Proceeding of the International Conference on Concrete Constructions, 2009, 187–194.
[8] M. Horstmann, J. Hegger, M. Zell, and C. Kulas, Large-sized building envelopes and slender shell structures made of TRC, in: Proceedings of the 8th International Symposium on Utilization of High-Strength and High-Performance Concrete, 2008, 1183–1190.
[9] M. Curbach, and S. Sheerer, Concrete light – Possibilities and visions, in: Proceedings of the fib Symposium Concrete Engineering for Excellence and Efficiency (Prague), 2011, 29–44.
[10] A. Magri, M. Colombo, and M. di Prisco, TRM and UHPFRC: retrofitting solutions for structural elements, in: Proceedings of the 3rd International Conference on Concrete Repair, Rehabilitation and Retrofitting, ICCRRR 2012, 2012, 1292–1297.
[11] V. Mechtcherine, Novel cement-based composites for the strengthening and repair of concrete structures, Constr. Build. Mater. 41 (2013) 365–373.
[12] V. Mechtcherine, Towards a durability framework for structural elements and structures made of or strengthened with high-performance fibre-reinforced composites, Constr. Build. Mater. 31 (2012) 94–104.
[13] Available at: <www.easee-project.eu> – EASEE – Envelope Approach to improve Sustainability and Energy Efficiency in existing multi-storey multi-owner residential buildings.
[14] T. Sharaf, W. Shawkat, A. Fam, Structural performance of sandwich wall panels with different foam core densities in one-way bending, J. Compos. Mater. 44 (2010) 2249–2263.

[15] L. Ferrara, M. Colombo, M. di Prisco, and C. Zecca, Sandwich panels with glass fiber reinforced surfaces for affordable housing, in: Proceeding of Challenges for Civil Constructions, Porto (Portugal), 2008.
[16] M. Colombo, M. di Prisco, and C. Zecca, On the coupling of soft materials with thin layers of glass fibre reinforced mortar, in: Proceeding of Challenges for Civil Constructions, Porto (Portugal), 2008.
[17] M. di Prisco, L. Ferrara, M. Lamperti, S. Lapolla, A. Magri, G. Zani, Sustainable roof elements: a proposal offered by cementitious composites technology, in: M.N. Fardis (Ed.), Innovative Materials and Techniques in Concrete Construction, Springer, The Netherlands, 2012, pp. 167–181.
[18] M. di Prisco, and G. Zani, Experimental and numerical analysis of advanced cementitious composites for sustainable roof elements, in: Proceedings of the Numerical Modeling – Strategies for Sustainable Concrete Structure, Aix-en-Provence (France), 2012.
[19] F. Muller, C. Kohlmeyer, and J. Schnell, Load-bearing behaviour of sandwich strips with XPS-core and reinforced HPC-facings, in: Proceedings of the 3rd International Symposium on Ultra-High Performance Concrete and Nanotechnology for High Performance Construction Materials (Kassel), 2012.
[20] European Standard EN 13163, Thermal insulation products for buildings – factory made products of expanded polystyrene (EPS) – specification, 2008.
[21] ASTM International C 578-92, Standard specification for rigid, cellular polystyrene thermal insulation.
[22] I.G. Colombo, A. Magri, G. Zani, M. Colombo, M. di Prisco, Textile reinforced concrete: experimental investigation on design parameters, Mater. Struct. 46 (2013) 1933–1951.
[23] European Standard EN 196-1, Method of testing cement – part 1: determination of strength, 2005.
[24] K. Stamm, H. Witte, Sandwichkonstruktionen: Berechnung, Fertigung, Ausfiihrung, Springer-Verlag, Wien, New York, 1974.
[25] W. Brameshuber, T. Brockmann, M. Curbach, C. Meyer, G. Vilkner, B. Mobasher, Peled, H.W. Reinhardt, M. Kruger, J. Wastiels, Concrete/matrix, in: W. Brameshuber (Ed.), Textile Reinforced Concrete – State-of-the-art Report of RILEM Technical Committee 201, RILEM Publications S.A.R.L., 2006, pp. 29–56.
[26] J. Hegger, N. Will, M. Curbach, F. Jesse, Load-bearing behaviour of Textile Reinforced Concrete. Bond cracking behaviour and load-bearing behaviour, Beton. Stahlbetonbau 99 (2004) 452–455.